ELSEVIER

Materials Science and Engineering A289 (2000) 276–288

MATERIALS SCIENCE & ENGINEERING A

www.elsevier.com/locate/msea

Mechanical properties and non-homogeneous deformation of open-cell nickel foams: application of the mechanics of cellular solids and of porous materials

X. Badiche [a], S. Forest [a,*], T. Guibert [a], Y. Bienvenu [a], J.-D. Bartout [a], P. Ienny [b], M. Croset [c], H. Bernet [d]

[a] *Ecole des Mines de Paris/CNRS, Centre des Matériaux/UMR 7633, BP 87 91003 Evry, France*
[b] *Ecole des Mines d'Alès, Laboratoire de Métrologie et Mécanique, 6 Av. de Clavières, 30319 Alès, France*
[c] *NiTECH, ZI du Clos Marquet, rue Michel Rondet, 42400 Saint-Chamond, France*
[d] *Suez Industrie, 68 rue du Fg Saint-Honoré, 75008 Paris, France*

Received 8 November 1999; received in revised form 9 February 2000

Abstract

The mechanical properties of open-cell nickel foams are investigated for the range of densities used in industrial applications for energy storage. The obtained Young's modulus, compression yield stress and tensile fracture stress are compared to the predictions of models based on periodic, Penrose and Voronoi beam networks. It is found that Gibson and Ashby's model [L.J. Gibson, M.F. Ashby, Cellular Solids, Cambridge University Press, Cambridge, 1998] provides the proper scaling laws with respect to relative density for almost all investigated properties. The strong anisotropy of the observed overall responses can also be accounted for. The two-dimensional strain field during the tension of a nickel foam strip has been measured using a photomechanical technique. Non-homogeneous deformation patterns are shown to arise. The same technique is used to obtain the strain field around a circular hole in a nickel foam strip. The observed deformation fields are compared to the results of a finite element analysis using anisotropic compressible continuum plasticity.

Keywords: Cellular solid; Porous material; Nickel foam; Strain field measurement; Anisotropic compressible plasticity; Penrose lattice

1. Introduction

Metal foams are used in many industrial applications ranging from thermal insulation, electromagnetic shielding, to energy absorption during car crash [1]. Nickel foams are well-suited for battery applications and are involved for instance in portable computers and mobile phones. This requires outstanding mechanical and electrical properties. The use of light and highly conductive foams leads to a considerable increase of the energy density, whereas a high tensile strength is necessary for smooth processing of the foam during the battery production steps like 'pasting', calendering and coiling. The nickel foam studied in this work is produced in the form of sheets or coils.

The design of an optimal foam for wanted mechanical and electrical properties requires a sound knowledge of the relation between microstructural parameters like density or number of cells or struts per unit volume and the effective properties. That is why linear properties like elasticity moduli (and electrical conductivity in appendix) and non-linear properties like yield and fracture strengths are investigated in this work for relative densities of industrial interest ranging from 0.01 to 0.05. These properties turn out to be strongly anisotropic and this anisotropy is mainly due to material processing. The deformation of heterogeneous highly porous materials often is associated with the development of non-homogeneous deformation patterns like strain localization, in the form of bands during the compression of aluminium foams for instance [2,3]. Although the deformation of nickel foam strips in tension does not lead to significant localization phe-

* Corresponding author. Tel.: +33-1-60763051; fax: +33-1-60763150.
E-mail address: samuel.forest@mat.ensmp.fr (S. Forest)

0921-5093/00/$ - see front matter
PII: S0921-5093(00)00898-4

nomena before initiation of a final crack and fracture, photomechanical measurement methods are used in this work to display the two-dimensional strain field during the test. Similar strain field measurement techniques, together with X-ray tomography, have been used for aluminium foams in [4]. The present results are given in Section 3 and reveal the existence of slightly inhomogeneous deformation patterns appearing at the very beginning of the test. A description of nickel foam processing, microstruture and of the experimental techniques used in this work is given in Section 2 and the experimental results are presented in Section 3. The electrical properties of the material are of the utmost importance for industrial applications. Since this work mainly focuses on mechanical properties of metal foams, the results on electrical conductivity measurements are given in appendix. It is shown that the electrical properties can be interpreted using the same type of models as for the mechanical properties.

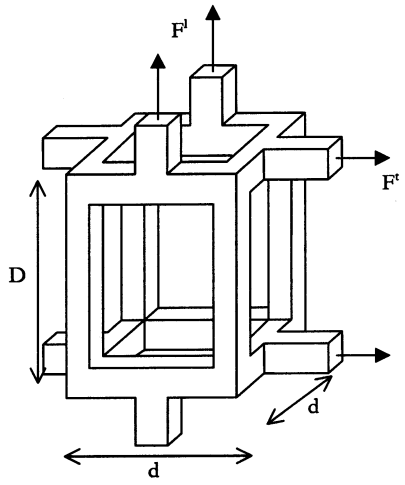

Fig. 1. Anisotropic idealized unit cell for the mechanical analysis of metal foams (after [5]).

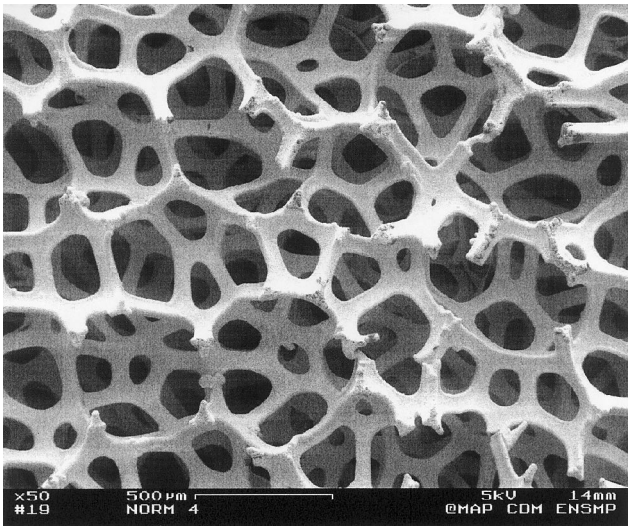

Fig. 2. Cellular structure of a nickel foam.

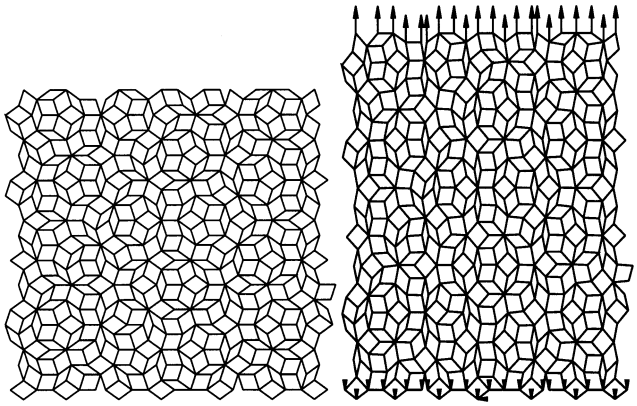

Fig. 3. Quasiperiodic Timoshenko beam network and its deformed state in tension for linear elasticity.

Two classes of material models are available to simulate and predict the response of metal foams under various loading conditions. The micromechanical approach relies on the knowledge of the behaviour of the constituent and of the cellular structure to derive the effective properties. Simple and efficient models can be found in [5] and apply for a wide range of foams. They are based on idealized cellular structures like grids or honeycombs in the two dimensional case. In the three-dimensional case, the idealized unit cell proposed in [5] can be used for instance to predict elastic properties and the plateau stress in compression. A straightforward extension exists accounting for anisotropic behaviour (Fig. 1 and [6]). As can be seen from Fig. 2, the cell distribution is actually non periodic, which strongly affects the effective non-linear properties for instance. For that purpose, random models for cellular materials have been introduced in [7], in the form of two-dimensional Voronoi honeycombs. Since the representative unit cell of the nickel foam rather is a pentagonal dodecahedron which cannot lead to periodic space tesselation [8,9], the case of quasiperiodic beam networks is introduced in this work and represents an intermediate model between periodic and random lattices. The example of a two-dimensional Penrose beam network and its elastic deformation in tension is given in Fig. 3.

The second class of constitutive models for metal foams is the phenomenological approach that leads to full three-dimensional models that can be implemented in finite element codes for structural applications. The main advantage of this approach is that it can account for non-homogenous deformation of structures made of metal foam. The mechanics of porous materials has been developed to describe the processing and constitutive behaviour of powder metallurgy materials [10] but also ductile fracture of materials (see, e.g. [11]). Although micromechanical arguments are available to construct three-dimensional compressible plasticity

criteria [12], the parameters appearing in these models can be identified phenomenologically from macroscopic tests. There is a need for simple and reliable engineering constitutive equations for metal foams. That is why the phenomenological approach has been used for aluminium foams in [13,14]. This is done in this work for nickel foams and the prediction capability is illustrated in the case of a nickel foam strip with a hole in tension. The two classes of models are confronted with experimental results in Section 4. One original aspect of this work is the use of an anisotropic plasticity criterion for which an identification procedure is applied, based on the measurement of length, width and thickness variations during uniaxial straining. The parameters of such models can also be identified using multiaxial tests like axisymmetric compression in [14]. But multiaxial homogeneous loading conditions are difficult to design for foam sheets.

2. Experimental procedures

The main features of nickel foam processing and of the obtained microstructure are described in this part and this is followed by a presentation of the different mechanical tests performed in this work.

2.1. Material processing and cellular structure

The production of nickel foams can be decomposed into five main steps [15]. A polyurethane foam having the thickness and the porosity of the final product is selected and covered with an electrically conductive coating. Nickel is then electroplated on the coated surface, before burning out the polyurethane foam. A final thermal treatment is necessary to obtain the wanted mechanical properties. The firm NiTECH has developed an original process for the second step, namely cathodic magnetron nickel sputtering, which allows the treatment of polyurethane of different thicknesses, from 1.2 to 6 mm and of different porosities. Impurities like carbon and sulphur are present in nickel after material processing, in contents lower than 100 and 50 ppm, respectively. The successive processing steps being continuous, the nickel foam sheets are submitted to a tensile force in the rolling direction called RD. The transverse direction will be denoted TD in the sequel.

The obtained cell structure is given on Fig. 2 where mainly dodecahedral cells with open pentagonal faces can be seen. The mean cell diameter is about 500 μm but can be varied from 400 μm to 1.2 mm depending on the final application. The structure of nickel foams is the quasi exact replication of that of the original polyurethane foam. In particular, the section of a strut typically is a so-called 'Plateau border' which corresponds to a structure controlled by surface tension and interfacial effects during the foaming of the polyurethane substrate and the explosion of the cell walls to get an open-cell foam structure. Since the polymer is eventually burnt out, the nickel struts are hollow. Typical length and diameter of a strut are 150 and 70 μm. The walls of the struts are about 10 μm thick. The roughness of the surface of the struts is due to the electroplating process. The final heat treatments lead to nickel grain sizes from 1 to 10 μm. The investigated properties will be shown to depend mainly on the relative density of the foam, defined as the ratio of the mass density of the cellular material and that of pure nickel:

$$\rho_* = \frac{\rho_{\text{foam}}}{\rho_{\text{Ni}}}, \text{ with } \rho_{\text{Ni}} = 8900 \text{ kg m}^{-3} \quad (1)$$

An other important parameter is the number n of struts in the thickness of the nickel foam sheet. This number must be large enough for the material to be considered homogeneous on a macroscopic scale. If it is too small, strain will tend to localize in some weaker section and homogeneous deformation of the foam will be impossible. This number is defined as the ratio between the thickness e and the mean strut length a. In this work, values of n from 6 to 18 have been studied. Other parameters like specific surface areas and tortuosity have been studied in [16] for very similar nickel foams.

2.2. Heterogenity and anisotropy

Several aspects of the material processing contribute to introduce a variability of the cell structure in the material. First of all, the thickness t_e of the deposited nickel layer at the surface of the foam is greater than the thickness t_i in the mid-section of the foam. The electroplating technique is intrinsically associated with a thickness deposition ratio ($\text{TDR} = t_e/t_i$) different from one. The obtained values of TDR range from 1.2 to 1.6. This may play an important role in the interpretation of the compression tests discussed in Section 3.2.

The foaming process of polyurethane gives rise to an elongation of the cells in the direction of gravity. Two cutting techniques are used to obtain the skeleton of the nickel foam. The peeling of parallelepipedic polyurethane foam blocks leads to a periodic variation of the structure of the peeled foam, since the elongated polyurethane cells are successively cut along their long and short axes. In contrast, the slit cutting of a long block of polyurethane gives a more uniform isotropic structure. Many results given in this work have been obtained for the latter product called LS (for loop-slitting). There is however another source of anisotropy for the final product and even for LS nickel foams, namely the tensile force applied to the foam during the

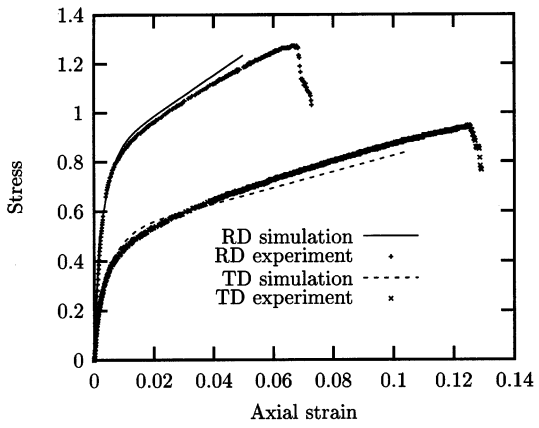

Fig. 4. Tensile behaviour of a nickel foam (LS foam with $\rho_* = 0.028$); the results of the simulation using the model developed in Sections 4.2 and 4.3 are also presented (stress in MPa).

processing. This results in cells that are more elongated in average in direction RD that in the transverse direction. Considering the idealized unit cell of Fig. 1, this anisotropy can be expressed by the aspect ratio:

$$R = \frac{D}{d} \tag{2}$$

where D is measured in direction RD. A typical value of 1.5 is deduced from the analysis of elastic properties (see Section 3.1) and electrical properties (see appendix). The resulting strong anisotropy of the overall material properties will be shown in the next sections.

2.3. Mechanical testing methods

An electro-mechanical machine with a load cell of 50 kg is used to perform tensile tests on nickel foam samples. The specimens are 200 mm long and 20 mm wide nickel foam strips. The thickness varies from 1.2 to 6 mm depending on the density of the studied foam. The specimen's ends are compressed in the tensile machine grips and deformation is measured using an extensometer clipped on the specimen. The directions RD and TD are carefully distinguished in the tests.

Nickel foams can be compressed in the direction normal to the sheet plane. In order to perform compression tests, disks of 20-mm diameter have been cut out of the nickel foam sheet. Due to the limited thickness of the specimen, only the relative displacement of the test machine platens can be measured. It has not been possible to significantly reduce friction between the specimen and the machine platens.

2.4. Photomechanical strain field measurement method

The use of an extensometer clipped on the sample gives no indication on the homogenity of deformation along the specimen. Morever the weight and rigidity of the extensometer itself may lead to some bias in the measurement of mechanical response of particularly thin foams. That is why a strain field measurement method has been used to investigate these different aspects of foam deformation.

Optical methods are well-suited for non-destructive testing because they are non-intrusive and do not affect the surface of the specimens [17]. The used optical extensometer provides a bidimensional field of in-plane displacements. When an optically rough surface is illuminated by light, the surface acquires a granular appearance. The porous surface of metal foams is particularly adapted for such observations. An imaging system (CCD camera) is used to record the successive states of a zone (or even the whole specimen) of the flat specimen under loading. Natural characteristic patterns arising from the surface roughness can be identified and followed during deformation thanks to digital image processing. The determination of displacements is based on digital image correlation (see [17]). Three components of the strain field are then deduced from the two-dimensional displacement field.

The idea of applying strain field measurement methods to cellular solids goes back to Chen and Lakes [18] who resorted to a holographic method. A similar speckle measurement method has been used in [3,4] for the study of closed-cell aluminium foams. However in the latter case, the cell size was not negligible when compared to the specimen size so that the discrete deformation of individual cells could be observed. In contrast, the size of the zone of the nickel foam specimen investigated here is large enough for the material to be regarded as statistically homogeneous and treated as a continuous medium. The continuous deformation fields observed in tension are reported in the next part.

The technique has been applied to tensile tests on nickel foam strips, extension tests (plane tension of wide strips leading to almost vanishing lateral deformation) and to the tension of a strip with a circular hole.

3. Results

The observed tensile and compressive properties of nickel foams are reported below, as well as the new insights brought by the use of photomechanical strain field measurement methods.

3.1. Tensile tests

Fig. 4 shows the material response to tensile loading conditions in both directions RD and TD. The final crack leading to fracture usually starts from one lateral boundary of the sample far from the grips. No significant dependence on material response and ductility of the way of cutting the samples out of the coils or sheets

has been noticed. The linear and non-linear tensile properties are successively reported.

The elastic part of the curve is hard to estimate so that unloading conditions have been prescribed at the beginning of the test in order to measure Young's modulus in both directions. The unloading curves of Fig. 5 exhibit a slight hysteresis loop but elastic moduli

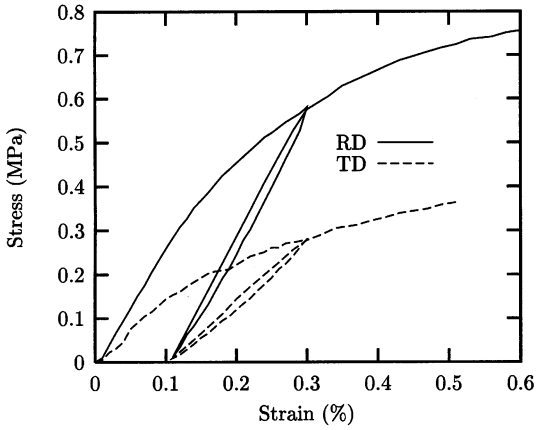

Fig. 5. Unloading condition at the beginning of a tensile test for the determination of Young's modulus in each direction (LS foam $\rho_* = 0.028$).

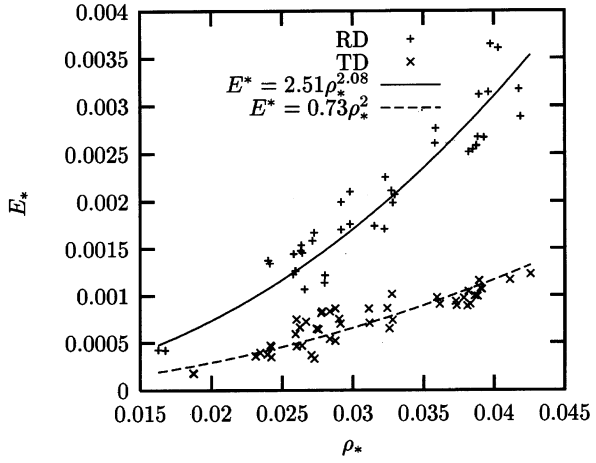

Fig. 6. Relative Young's modulus as a function of relative density.

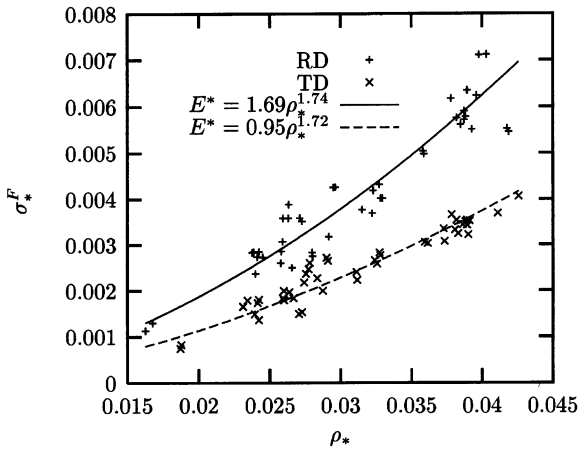

Fig. 7. Relative fracture stress in tension as a function of relative density.

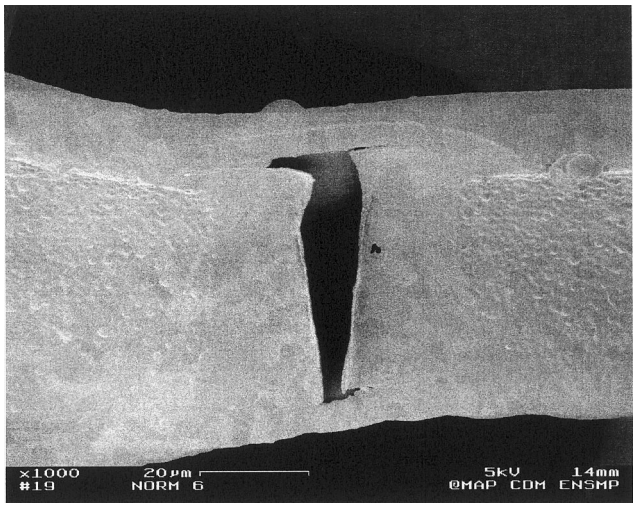

Fig. 8. Failure of a nickel strut: cracks develop at the boundary between the wall and the edges of the Plateau border that exhibit a mass excess due to the electroplating process.

can be unambiguously determined and display a strong anisotropy. The relative Young's modulus in each direction is given as a function of relative density on Fig. 6 and is defined by

$$E_* = \frac{E_{\text{foam}}}{E_{\text{Ni}}} \text{ with } E_{\text{Ni}} = 214 \text{ GPa} \quad (3)$$

E_{Ni} for bulk isotropic nickel. The Poisson ratio could not be measured using this technique and the problem of transverse deformation is tackled in Section 3.3 using photomechanics. It must be noted that the elastic properties vary with deformation. For a LS foam (with $\rho_* = 0.028$), Young's modulus in direction RD increases from 300 MPa at 0.3% strain to 360 MPa at 5%. In direction TD Young's modulus goes from 150 Mpa at 0.3% to 200 MPa at 10%. The Young's modulus is found to increase very sligthly with n, the number of struts through the thickness.

The elastoplastic response of nickel foams shown on Fig. 4 displays a very low initial yield stress, a non-linear regime followed by almost linear hardening. The stress is computed using the prescribed force and the initial section of the specimen, whereas the reported strain is the ratio between the specimen elongation and the initial gauge length. The nickel foams exhibit a strongly anisotropic elastoplastic behaviour: the ductility in direction TD is almost twice that in direction RD. The maximum stress reached before fracture is plotted as a function of relative density in Fig. 7. An example of a fracture process in a strut can be seen on Fig. 8, where the role played by the Plateau border shape clearly appears. At the level of the nickel strut, fracture is intergranular as shown on Fig. 9. The embrittlement of grain boundaries can likely be attributed to the presence of sulphur in the material.

3.2. Compression tests

Some compression curves are presented on Fig. 10. Several features of these curves are common to many cellular solids under compression: a plateau is reached after an almost linear regime and followed by a pronounced hardening stage corresponding to nickel densification. The short plateau at the very beginning of the curves may be attributed to defects in the flatness of the specimens mainly due to the deformation induced by the machining. In general, the curves display a peak followed by apparent softening or a short plateau. A similar behaviour can be observed on polymer foams [6]. The peak tends to disappear for foams with rather small n and therefore large cells. Interrupted tests before, at and after the peak followed by SEM observations have shown that the hinge deformation mechanism proposed in [5] applies here and starts at the peak. Observations on homogenity of deformation within the thickness during the test were not possible but interrupted tests indicate that the slightly less dense core of the sheet (due to the existence of a TDR different from 1) fails earlier.

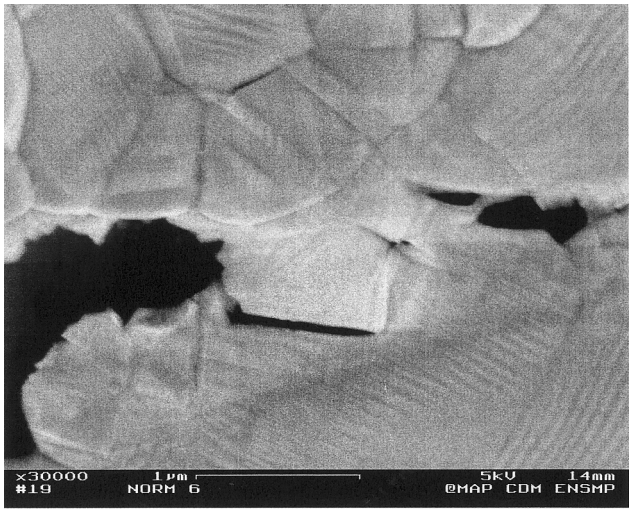

Fig. 9. View of a crack tip in a nickel wall: intergranular crack propagation.

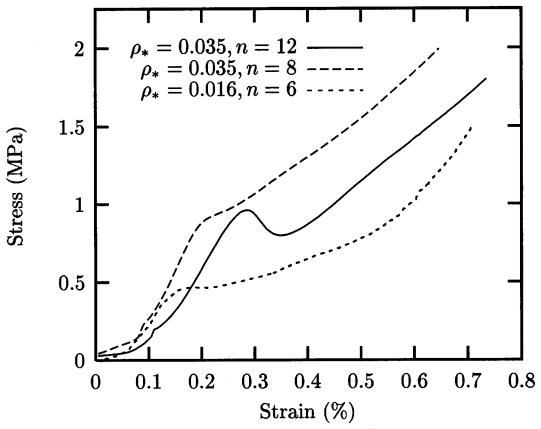

Fig. 10. Compression tests on nickel foams with different relative densities and numbers of cells within the thickness.

3.3. Strain distribution during a tensile test

The photomechanical technique enables one to compute the components ε_{11},ε_{22} and ε_{12} of the strain field during the deformation of a nickel foam strip in tension along direction 2 (which will be RD or TD in the following tests). In particular, averaged values of ε_{11} can be computed over a central part of the sample in order to have access to transverse deformation. The ratio $-\varepsilon_{11}/\varepsilon_{22}$ of transverse versus longitudinal deformation is found to be not far from 0.5 when the tensile direction 2 coincides with RD, whereas a very different result, namely about 0.25, is obtained for the other direction. This confirms the very strong anisotropy of the behaviour of nickel foams. Precise measurements in the elastic regime for the determination of Poisson ratios for each direction are still to be performed.

Deformation maps of a LS nickel foam in tension along RD are presented on Fig. 11 for a global deformation of about $\varepsilon_{22} = 6.5\%$. The strain field turns out to be relatively inhomogoneous and this has been observed on the 12 specimens of various densities that have been investigated using the photomechanical technique. A fluctuation $\Delta\varepsilon_{22}$ equal to about 1.8% develops at the very beginning of deformation and remains almost constant during further deformation. Some band-like deformation patterns are generally observed but the crack leading to final fracture does not systematically appear within them. A similar heterogenity in transverse deformation exists. The effects of the grips at the sample ends where the transverse deformation is constrained to be nearly zero, can be seen on Fig. 11(b) since the whole gauge length has been analysed. Note that the obtained heterogenity cannot be explained only by some variations of the specimen thickness. The initial thickness of the sample was measured and found to vary from 1.95 to 2.05 mm. A finite element analysis, similar to the simulations to be reported in the discussion, has been carried out including random variations of specimen thickness: maximal fluctuations $\Delta\varepsilon_{22}$ of about 0.1% have been obtained. On the other hand, the observed heterogeneous deformation patterns cannot be related to edge effects mentioned in [19]. Different cutting techniques of the specimens have been used and do not affect significantly the deformation of the samples considered here. However, the observed heterogenities remain small and stable enough, so that they do not significantly affect the overall properties determined in the previous sections.

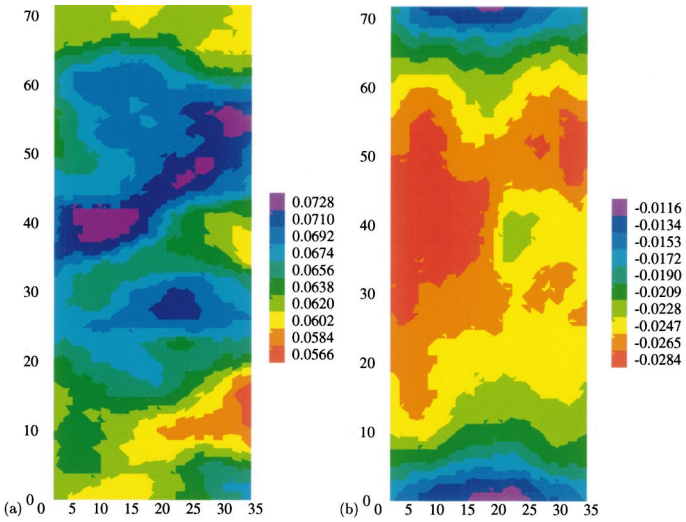

Fig. 11

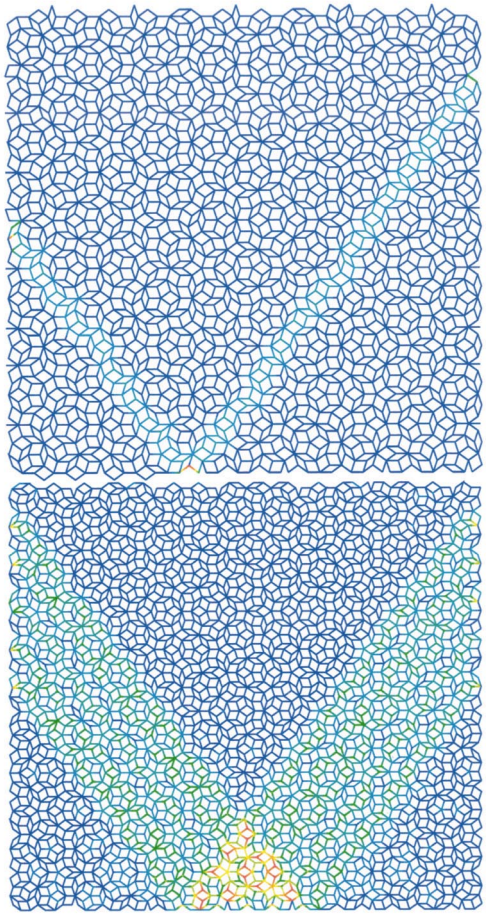

Fig. 14

Fig. 11. Strain field measurements on a nickel foam in tension: axial strain ε_{22} (a) and transverse strain ε_{11} (b); distances are given in mm, the tensile direction is the vertical one and coincides with RD; $\rho_* = 0.025$.

Fig. 14. Strain localization (above) and deformation band propagation (below) in an elastoplastic quasi-periodic beam network in tension along the vertical direction; equivalent plastic deformation in the beams; the deformation within the band is about 10 time larger than in the surrounding material and saturates at 2% before the next band starts.

3.4. Deformation maps of a foam sheet with a circular hole in tension

Metal foams are used in industrial structures with specific geometries that may lead to non-homogeneous deformation during straining of the component. As an example of simple structure, we consider a 124-mm long and 50-mm large nickel foam strip with a circular hole, 25.5 mm in diameter, at its center. When submitted to tensile loading conditions at its ends, a non-homogeneous strain field develops that can be recorded using the photomechanical technique. The two strain components along the ligaments of the specimen (from the notch to the free boundary) are given on Fig. 12 and Fig. 13 together with the finite element simulations provided at the end of next part. The results are given for tension in RD for 0.3% overall deformation. The tests have been carried out in direction TD too, but the results are not provided for conciseness. Note that significantly higher strains are reached at the notch for tension in direction TD than in direction RD.

4. Discussion and constitutive modelling

The micromechanical and phenomenological approaches of the mechanics of cellular solids are successively applied to interpret the previous experimental results and to predict the overall and structural non-linear mechanical properties of nickel foams.

4.1. Linear and non-linear beam models

4.1.1. Young's modulus

Predictions of Young's modulus for cellular solids can be derived from the models based on beam networks presented in the introduction. They are reported in Table 1. The predicted relative Young modulus is found to be proportional to ρ_*^m where the exponent m strongly depends on the retained unit cell [20,21]. A linear relationship is found if the struts are regarded as bars carrying only normal forces, whereas powers 2–3 are expected if the bending of beams is introduced. Note that the Penrose lattice proposed in this work leads to a power not far from that obtained in the case of random networks. However the chosen quasi-periodic lattice does not respect the geometric properties of the structure of the present foam, in particular the number of edges ending at a given node, but a more realistic network should be three-dimensional.

The experimental results are compatible with Gibson and Ashby's model [5] for both directions RD and TD as can be seen on Fig. 6. The use of the anisotropic unit cell of Fig. 1 [6,22] leads to the following expression of the ratio between the predicted longitudinal and transverse Young's moduli:

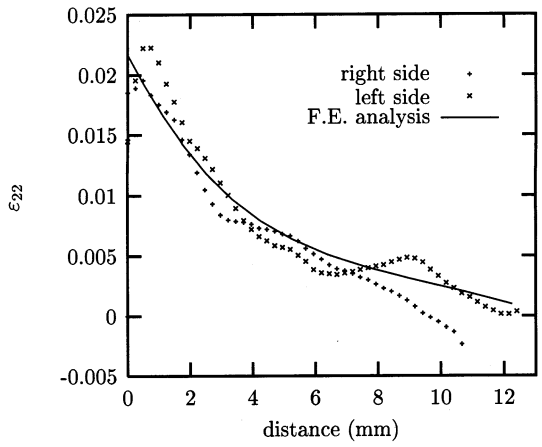

Fig. 12. Axial deformation along a horizontal line (ligament) starting from the notch; tensile direction 2 coincides with RD; distance from the hole in mm (overall deformation of 0.3%)

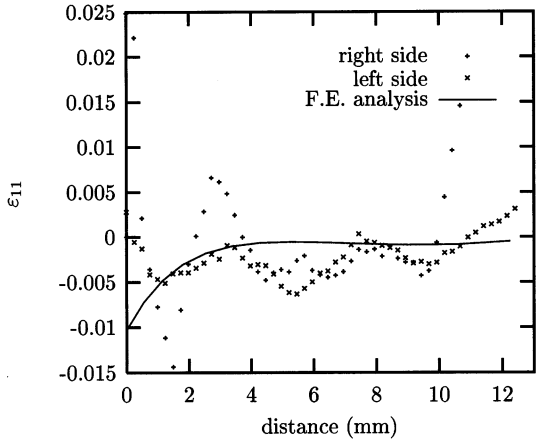

Fig. 13. Lateral deformation along the ligament starting from the notch; tensile direction 2 coincides with RD; distance from the hole in mm (overall deformation of 0.3%)

$$\frac{E_*^{RD}}{E_*^{TD}} = \frac{2R^2}{1+R^{-3}} \tag{4}$$

Experimentally, $E_*^{RD}/E_*^{TD} \simeq 3.45$, which implies $R \simeq 1.5$. Note that a similar simple beam model exists to predict the electrical conductivity of the foam (see Appendix) and is compatible with the same value of the aspect ratio.

4.1.2. Hardening behaviour and localization phenomena

The extension of the beam network models to account for the non-linear regime requires the knowledge of the non-linear mechanical response of the constituent. The determination of the elastoplastic behaviour of a nickel strut is a challenging problem that has been tackled in [23]. For that purpose, the tensile behaviour of nickel films of 400 μm thickness which have been submitted to the same heat treatments as the nickel foams, has been determined. The measured elastic properties significantly differ from the usual ones mentioned in textbooks due to the texture of the films and to the fact that a nickel film is a multicrystalline material with sometimes only one grain through the thickness. These results and the constitutive modelling of elastoplastic pure nickel have been reported in [23]. They have been used to compute the non-linear response of periodic and random beam networks and to compare it with experimental results. A good agreement has been obtained at least under uniaxial loading conditions. In contrast, we report here the very specific non-linear response of the quasi-periodic lattice. The tensile behaviour of the Penrose network of Timoshenko beams of Fig. 3 is considered again but an elastoplastic behaviour with non-linear isotropic hardening is attributed to each beam. The deformation maps of Fig. 14 show that deformation immediately tends to localize within deformation bands. Once a band has formed, deformation further proceeds by localization band propagation spreading over the entire specimen. The inclination of the bands of about $\pi/5$ (36°) with respect to the tensile direction reflects the underlying quasi-periodic structure of the network. Note that this angle is close to the orientation of shear bands in an isotropic incompressible elastoplastic medium under plane stress conditions (namely 35.26°). In contrast, periodic structures like grids and honeycombs have not been found to be prone to localization phenomena, at least under tensile conditions. Shear bands in Voronoi honeycombs under compression have been simulated in [7] but the tensile case remains to be considered. This propensity of quasi-periodic lattices to strain localization may perhaps explain to some extent the observed systematic strain heterogenity in tension (see Section 3.3) but the more realistic 3D extension remains to be done.

4.1.3. Fracture stress in tension

The maximum stress reached before fracture is plotted as a function of relative density in Fig. 7. A strong

Table 1
Prediction of relative Young's modulus using periodic and non-periodic beam networks

	Hexagonal honeycomb	Gibson and Ashby [5]	Warren and Kraynik [26]	Bernet [23]	Voronoi honeycomb [7]	Penrose network
E_*	$\frac{3}{2}\rho_*^3$	$\approx \rho_*^2$	$3.2\rho_*^2$	$\frac{\rho_*}{6}$	$0.56\rho_*^{2.43}$	$2.6\rho_*^{3.44}$

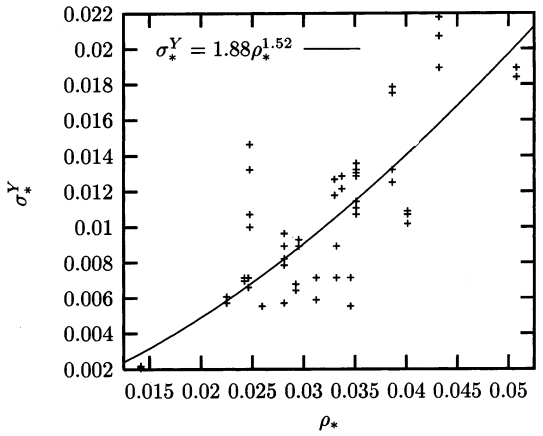

Fig. 15. Plateau stress of nickel foams under compression.

correlation seems to exist involving a power 1.7–1.75 of the relative density. In contrast, no correlation could be found between deformation before fracture and relative density. A model accounting for the found relationship between fracture stress and density remains to be developed, since no corresponding result has been found in literature yet.

4.1.4. Plateau stress in compression

When plotted as a function of relative density (Fig. 15), the stress reached at the plateau or at the peak is found to follow the power law ($m = 1.5$). This relationship is compatible with the hinge model proposed in [5]. The dispersion of the results is however more pronounced than for the properties previously investigated.

4.2. General constitutive framework based on the mechanics of porous media

The main drawback of the previous approach is that it can generally not provide a fully three-dimensional constitutive model to be used for structural calculations. That is why we resort here to a classical phenomenological constitutive framework based on continuum plasticity theory. The validity of such a continuum approach will be tested in the case of the nickel foam strip with a hole in tension. Metal foams being porous compressible materials, a compressible plasticity model originally proposed in [12] is retained and is similar to the one used in the work [10] dealing with powder metallurgy. An additional feature of the model is the introduction of plastic anisotropy as observed experimentally. Note that the model can be formulated within the framework of small deformations since the ductility in tension of the nickel foam is sufficiently low. The general form of the anisotropic elliptical plasticity criterion reads:

$$f(\underline{\underline{\sigma}}) = \left(\frac{3}{2}C(as_{11}^2 + bs_{22}^2 + cs_{33}^2 + 2(ds_{12}^2 + es_{23}^2 + fs_{31}^2)) + F(u\sigma_{11} + v\sigma_{22} + w\sigma_{33})^2\right)^{1/2} - R \quad (5)$$

where $\underline{\underline{s}}$ is the deviator of the stress tensor $\underline{\underline{\sigma}}$. This represents the anisotropic generalization of the quadratic criterion used in [14] for which parameters a–f and u, v, w are set to 1. A similar anisotropic extension of the Drucker–Prager criterion and the more general ones proposed in [13] is also possible. The components of these tensors are given with respect to the frame associated with the orthotropy axes of the foam. The ratio C/F accounts for the respective influence of the deviatoric and spherical parts of the stress on plastic yielding, whereas parameters a–f and u–w account for the anisotropic response. Plastic flow follows from assumed normality rule:

$$\dot{\underline{\underline{\varepsilon}}}^p = \dot{p}\,\frac{\partial f}{\partial \underline{\underline{\sigma}}} \quad (6)$$

where $\dot{p}$ is the plastic multiplier. An associated flow rule is also assumed in [13,14]. The expression of the plastic multiplier is the following in the isotropic case:

$$\dot{p} = \left(\frac{2}{3C}\dot{\underline{\underline{\varepsilon}}}_{dev}^p : \dot{\underline{\underline{\varepsilon}}}_{dev}^p + \frac{1}{9F}(tr\dot{\underline{\underline{\varepsilon}}}^p)^2\right)^{1/2} \quad (7)$$

where $\dot{\underline{\underline{\varepsilon}}}_{dev}^p$ denotes the deviatoric part of the plastic deformation tensor. In the general case, a viscoplastic framework is used according to which:

$$\dot{p} = \left\langle \frac{f(\underline{\underline{\sigma}})}{K} \right\rangle^N \quad (8)$$

where MacCauley brackets and viscosity parameters K, N have been introduced. Large values of N and small values of K lead to the rate-independent elastoplastic case considered in present work.

The non-linear work-hardening behaviour of the foam is described by the following hardening rule:

$$R = R_0 + Q(1 - e^{-Bp}) + Hp \quad (9)$$

which involves 4 parameters, R_0 being the initial threshold. The coefficients (Q, B) and H, respectively account for the non-linear initial and linear final parts of the tensile curves. This model is implemented in the finite element code Z-set described in [24]. Fully implicit global resolution and local integration schemes are used.

4.3. Parameter identification

The identification of the numerous parameters appearing in the anisotropic function and in the evolution equations requires sufficient experimental information.

Table 2
Material parameters of the anisotropic compressible plasticity model for a LS foam with $\rho_* = 0.028$

C	a	b	c	F	u	v	w	R_0 (MPa)	Q (MPa)	B	H (Mpa)
1.0	0.42	2.07	2.0	0.0018	1.0	20.6	23.3	0.45	0.37	3.3	8.17

When no multiaxial test is available, it is possible to identify some parameters from the knowledge of the stress-strain tensile curve and from the apparent Poisson ratio [13]. In the present anisotropic case, we have to consider at least two tensile tests in two different directions (here RD and TD) and to measure both lateral deformation components during the unaxial test. That is why the variations of the width and thickness of the tensile specimens have been recorded and used in the identification procedure. The criterion (Eq. (5)) leads to the following ratio of the yield stress in direction 1 and 2:

$$\left(\frac{\sigma_Y^1}{\sigma_Y^2}\right)^2 = \frac{C(a+4b+c)+6Fv^2}{C(4a+b+c)+6Fu^2} \tag{10}$$

The ratio of lateral versus longitudinal plastic deformation for tension tests in direction 1 is a consequence of application of normality rule (Eq. (6)):

$$\frac{\varepsilon_{22}^p}{\varepsilon_{11}^p} = \frac{C(-2a-2b+c)+6Fuv}{C(4a+b+c)+6Fu^2} \tag{11}$$

$$\frac{\varepsilon_{33}^p}{\varepsilon_{11}^p} = \frac{C(-2a+b-2c)+6Fuw}{C(4a+b+c)+6Fu^2} \tag{12}$$

Two similar relations hold for tension in direction 2. The criterion (Eq. (5)) can be multiplied by any constant so that the product Ca is arbitrary. In Eqs. (10)–(12), F, u, v, w are not independent and the actual unknowns are Fu^2, v/u, w/u, so that we can fix for instance $u = 1$. Five unknowns remain b, c, F, v, w that can be unambiguously determined using the previous five equations. However, due to experimental scatter, we do not directly solve these equations but rather resort to an optimization procedure based on a Levenberg–Marquardt algorithm and a quadratic cost function to determine a set of parameters describing experimental data with sufficient accuracy. The parameters R_0, Q, B and H appearing in the nonlinear hardening rule $R(p)$ are also included in this optimization loop in order to reproduce at best the whole tensile curves.

In contrast, in the available experimental data, there is not the necessary information to determine the parameters d–f characterizing shear anisotropy. Accordingly, shear isotropy $d = e = f = 1$ is assumed in the following. The importance of this assumption can be estimated in the structural analysis of next section.

The anisotropic elastic behaviour must also be taken into account. Some components of the orthotropic elasticity matrix can be identified. The remaining constants and in particular the shear moduli are estimated according to Voigt's approximation of homogenization theory [21].

The coefficients of the constitutive equations can be assumed to be constant since foam density does not vary significantly in the considered tensile tests. The identification of the material parameters has been performed for a LS foam (with $\rho_* = 0.028$) using the following experimental basis: tensile tests in direction RD and TD. The information about the transverse deformation in both tests (obtained by photomechanical analysis) thickness reduction has been taken into account in the identification procedure. The results of the parameter identification are shown on Fig. 4 and the parameters are given in Table 2. Note that the identification concerns only the tensile domain of the stress space, compression results have not been included, which would probably leads to a more sophisticated model [13].

The predictive capabilities of the model have been tested using extension tests for which wide specimens with a short gauge length are used in order to impose almost vanishing transverse deformation ($\varepsilon_{11} \simeq 0$) at least in a large part of the specimen. This gives rise to slightly higher stresses as shown on Fig. 16 that are correctly reproduced by the model using the parameters identified from tensile tests.

Note that the parameters obtained for the hardening rule Eq. (9) are not those of the behaviour of pure nickel. Such an approach may be possible but in this case C cannot be taken equal to 1 as done here. In the

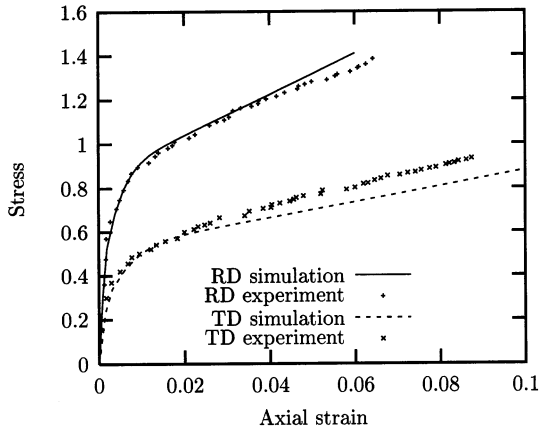

Fig. 16. Simulation of the extension (plane tension) of nickel foams in directions RD and TD; confrontation with experiment.

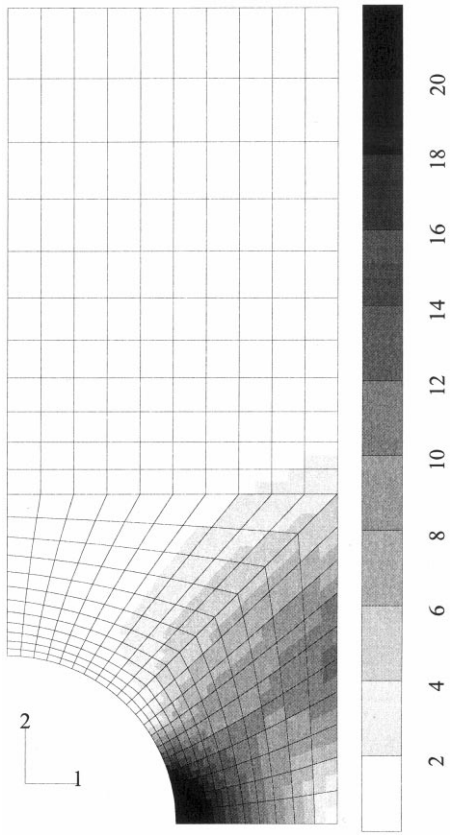

Fig. 17. F.E. simulation of the tensile deformation of a nickel foam plate with a hole: ε_{22} strain field (in %); direction coincides with TD.

literature of the mechanics of porous media, relationships between parameters C, F and the relative density have been derived considering for instance ideal arrangements of spheres or cylinders [12] or cubic networks. One of them [12] reads for instance:

$$C=\left(\frac{3-2(1-\rho_*)^{1/4}}{3(1-(1-\rho_*)^{1/3})}\right)^2, \quad F=\frac{1}{4(\log(1-\rho_*))^2} \qquad (13)$$

These formula are usually applied to higher densities than for metal foams but it is interesting to extrapolate them to the densities considered in this work. For instance, formula (Eq. (13)) leads in our case to a ratio C/F of 4.2 for $\rho_*=0.03$. This is in relatively good agreement with the value 5.6 of the corresponding indicative ratio $C(a+b+c)^2/(F(u+v+w)^2)$ that can be defined for the present anisotropic model, using the parameters of Table 2.

4.4. Application to the deformation of a foam plate with a hole

To check the validity of the previous continuum plasticity model, it is applied to the simulation of the deformation of a foam plate with a circular hole. The results are compared to experimental photomechanical measurements. A finite element simulation of the tests has been performed under plane stress conditions and the obtained deformed state is shown on Fig. 17. Deformation is not maximum on the ligament but rather in an inclined band starting from the equator and that tends to develop. This is due to the strongly anisotropic material behaviour. In experiment, final cracking is actually found to occur in such an inclined band (slightly less than 45° from the tensile axis). Quantitative comparison between experiment and simulation is illustrated here by the strain components obtained along the ligament of the sample. Only one fourth of the specimen is represented in the simulation for symmetry reasons, whereas experimental information about the two ligaments are reported. The measured components ε_{22} and ε_{11} along the ligament are compared with the finite element results on Figs. 12 and 13 for RD tensile test. The corresponding results for TD tensile test are available but they are not given here for conciseness. The model properly describes the mean variation of the strain field in both cases, although important fluctuations are observed experimentally that cannot be accounted for by the deterministic continuum plasticity approach. The origin of the fluctuations remains unclear but they are in accordance with the development of heterogenity during a tensile test on a homogeneous sample reported in Section 3.3. The strongly anisotropic response is correctly described by the numerical analysis. Note that shear component σ_{12} of the stress remains significantly smaller than the components σ_{11} and σ_{22} in the computation, which explains why the crude hypothesis of isotropic elastic and plastic shear properties does not alter the prediction.

Structural tests like compression of samples with a hole have already been performed on aluminium foams (see [3,25]) but strain field measurements combined with finite element analyses are well-suited tools to interpret them.

5. Conclusions

Non-homogeneous deformation seems to be an important feature of the mechanical behaviour of metal foams. Strain localization phenomena have been repeatedly observed in the compression of closed-cell aluminium foams [2–4]. In the tensile deformation of nickel foams, slightly non-homogeneous deformation patterns have been detected using photomechanical techniques. The ultimate strain at fracture being a major request of the users of the nickel foam product, a precise knowledge of the heterogeneous deformation patterns that may arise during a characterization test is an important information. Beam models for open-cell foams have been shown to provide good estimates of the overall properties of nickel foams or at least the

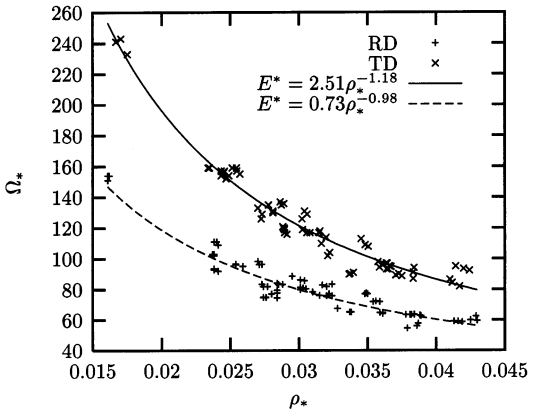

Fig. 18. Relative electric resistivity as a function of relative density.

correct dependency of these properties on relative density for the investigated range. However, in the non-linear regime, the available models are much less numerous. The proposed quasi-periodic beam model for instance is not adequate for nickel foams, since it is much more prone to localization than the actual material, at least for the two-dimensional version of the model investigated here. Furthermore, the prediction of two-dimensional strain fields in structures made of metal foam requires a full three-dimensional elastoplastic model. Compressible continuum plasticity has been shown to be a well-suited tool for this purpose, although material parameters must be identified for each given density. The proposed purely phenomenological approach represents a pragmatic way for computing industrial components involving metal foams using conventional finite element codes for which similar compressible plasticity models are already available. Improvements of the beam or continuum models are necessary to describe the observed compression behaviour.

A combination of the micromechanical and phenomenological approaches with a view to deriving relations between the parameters entering compressible plasticity criteria and material relative density surely represents the most promising framework for the general modelling of metal foam behaviour. The modelling of crack propagation then requires the introduction of damage mechanisms into this framework in a way similar to the treatment of ductile fracture of metals [11]. This further work is under progress.

Acknowledgements

R. Descamps and Ch. Bourgin, during their training period (Engineering degree at Ecole des Mines de Paris, speciality Engineering Materials) have contributed to the first stages of this study. The authors thank Professor A. Pineau for stimulating discussions and his help during the preparation of the manuscript. The authors thank the referees for drawing their attention on references [4] (that appeared during the reviewing procedure) and [14]. The second author thanks Professor N.A. Fleck for providing the manuscript [14] prior to publication.

Appendix A. Electrical conductivity of nickel foams

An electrical current of given intensity has been passed through ($L = 120$-mm) long and ($l = 20$-mm) wide nickel foam strips and the necessary tension has been measured in order to obtain the resistance r and associated resistivity Ω of nickel foam in a given direction:

$$\Omega = r\frac{le}{L} \tag{14}$$

The obtained relative resistivity $\Omega_* = \Omega/\Omega_{\mathrm{Ni}}$ with $\Omega_{\mathrm{Ni}} = 6.9 \times 10^{-8}\,\Omega$m for pure nickel, is plotted in Fig. 18 as a function of relative density of the foam and for both directions RD and TD. The observed relationship can be accounted for using a simple model of the foam based on a quadratic network which is a three-dimensional anisotropic extension of the square lattice. The length (direction RD) and width (direction TD) of the quadratic unit cell are denoted D and d respectively, similarily to Fig. 1. The predicted resistivity in both directions is:

$$\Omega_*^{\mathrm{RD}} = \frac{1+2/R}{\rho_*} \text{ and } \frac{\Omega^{\mathrm{RD}}}{\Omega^{\mathrm{TD}}} = \frac{1}{R} \tag{15}$$

In the isotropic case, this model gives the result $\Omega_*^{\mathrm{RD}} = 3/\rho_*$, which is not far from more sophisticated estimations like in [27,28]. If the previous model applies, the ratio of the observed longitudinal and transverse resistivities implies $R \simeq 1.5$, which is consistent with the result obtained for anisotropic elasticity.

The resistivity of nickel foams is found to be almost independent of n.

References

[1] Innovation 128, Les matériaux en mousse et leurs applications industrielles, Techtendances, Etudes Technologiques, Paris, 1998.
[2] Y. Chastel, E. Hudry, S. Forest, C. Peytour, Mechanical behaviour of aluminium foam for various deformation paths, in: J. Banhart, M.F. Ashby, N.A. Fleck. (eds.), Experiment and Modelling, Metal Foam and Porous Metal Structures, Verlag MIT Publishing, 1999, pp. 263–268. Journées d'Automne de la SF2M, Paris, 1998.
[3] K.Y.G. McCullough, N.A. Fleck, M.F. Ashby, Acta Mater. 47 (1999) 2323–2330.
[4] A.F. Bastawros, H. Bart-smith, A.G. Evans, J. Mech. Phys. Solids 48 (2000) 301–322.

[5] L.J. Gibson, M.F. Ashby, Cellular Solids, 1st edition, Cambridge University Press, Cambridge, 1998.
[6] A.T. Huber, L.J. Gibson, J. Mater. Sci. 23 (1988) 3031–3040.
[7] M.J. Silva, L.J. Gibson, Int. J. Mech. Sci. 39 (1997) 549–563.
[8] B. Grünbaum, G.C. Shephard, Tilings and Patterns, W.H. Freeman, San Francisco, CA, 1986.
[9] C. Janot, Quasycristals a Primer, Clarendon Press, Oxford, 1992.
[10] J. Besson, M. Abouaf, Mater. Sci. Eng. A 109 (1989) 37–43.
[11] A. Pineau, Effect of inhomogeneities in the modelling of mechanical behaviour and damage of metallic materials, 7th International Conference on Mechanical Behaviour of Materials, ESIS, The Hague, The Netherlands, 1995, pp. 1–22.
[12] R.J. Green, Int. J. Mech. Sci. 14 (1972) 215–224.
[13] R.E. Miller, Int. J. Mech. Sci. 42 (2000) 729–754.
[14] V.S. Deshpande, N.A. Fleck, J. Mech. Phys. Solids (2000) in press.
[15] M. Croset, W. Pruyn, Nickel Foam for High Performances NiCd and NiMH Batteries, CIBF, Beijing, 1997.
[16] A. Montillet, J. Comiti, J. Legrand, J. Mater. Sci. 27 (1992) 4460–4464.
[17] F. Laraba-Abbes, P. Ienny, R. Piques, Kautsch. Gummi Kunstst. 52 (1998) 209–214.
[18] C.P. Chen, R.S. Lakes, J. Mater. Sci. 26 (1991) 5397–5402.
[19] R. Brezny, D.J. Green, J. Mater. Sci. 25 (1990) 4571–4578.
[20] J.L. Grenestedt, Int. J. Solids Struct. 36 (1999) 1471–1501.
[21] S. Torquato, L.V. Gibiansky, M.J. Silva, L.J. Gibson, Int. J. Mech. Sci. 40 (1998) 71–82.
[22] S.V. Kanakkanatt, J. Cell. Plast. 9 (1973) 50–53.
[23] Ch. Bourgin, Th. Guibert, J.-D. Bartout, Y. Bienvenu, S. Forest, H. Bernet, M. Croset, Caractérisation et modélisation du comportement mécanique des mousses de nickel, Colloque National de Métallurgie des Poudres, SF2M, Commission de Métallurgie des Poudres et Frittage, Grenoble, 6–8 April, SF2M ed., 1998, pp. 41–48.
[24] J. Besson, R. Foerch, Comp. Methods Appl. Mech. Eng. 142 (1997) 165–187.
[25] A. Paul, T. Seshacharyulu, U. Ramamurty, Scripta Mater. 40 (1999) 809–814.
[26] W.E. Warren, A.M. Kraynik, J. Appl. Mech. 55 (1988) 341–346.
[27] A.K. Datye, R. Lemlich, Int. J. Multiph. Flow 9 (1983) 627–636.
[28] R. Lemlich, J. Colloid Interface Sci. 64 (1978) 107–110.